

Article

Numerical Study on Failure Mechanisms of Deep Roadway Sidewalls with Different Height-Width Ratios and Lateral Pressures

Xingzhong Wu ¹, Yubao Zhang ^{1,2,*} , Minglu Xing ^{1,2}, Bo Jiang ¹ and Jianye Fu ¹

¹ College of Energy and Mining Engineering, Shandong University of Science and Technology, Qingdao 266590, China

² State Key Laboratory of Mining Disaster Prevention and Control Co-Founded by Shandong Province and the Ministry of Science and Technology, Shandong University of Science and Technology, Qingdao 266590, China

* Correspondence: yubao.zhang@sdust.edu.cn

Abstract: The stability of roadway sidewalls is crucial to ensuring people's safety and production efficiency in coal mining. This paper investigated the deformation and failure of deep roadway sidewalls, particularly the effects of height-width ratios and lateral pressure coefficients. Our research results indicate that brittle failure occurred in the diabase sidewall rock of the Datai coal mine, and a V-shaped pit was formed as a result of shear damage caused by high stress. When the height-width ratio of a roadway increases from 0.25 to 2.00, the tensile and shear plastic failure area of the sidewall increases, and vertical stress is transferred to a deep part of the roadway sidewall. There are two stress concentration zones and two stress peak points in the sidewall of a roadway. When the lateral pressure coefficient increases from 0.10 to 1.00, the tensile plastic zone of rock mass in the sidewall first decreases and gradually reaches stability. On the other hand, the shear failure area increases and then decreases. Similarly, the sidewall horizontal displacement decreases and then increases. Additionally, the vertical stress concentration position is located near the roadway sidewall.

Keywords: roadway sidewall stability; high in-situ stress; brittle failure; height to width ratio; lateral pressure coefficient



Citation: Wu, X.; Zhang, Y.; Xing, M.; Jiang, B.; Fu, J. Numerical Study on Failure Mechanisms of Deep Roadway Sidewalls with Different Height-Width Ratios and Lateral Pressures. *Appl. Sci.* **2024**, *14*, 3892. <https://doi.org/10.3390/app14093892>

Academic Editor: Nikolaos Koukourzas

Received: 19 March 2024

Revised: 28 April 2024

Accepted: 29 April 2024

Published: 1 May 2024



Copyright: © 2024 by the authors. Licensee MDPI, Basel, Switzerland. This article is an open access article distributed under the terms and conditions of the Creative Commons Attribution (CC BY) license (<https://creativecommons.org/licenses/by/4.0/>).

1. Introduction

After excavation, the stress state of the surrounding rock changes dramatically and stress is redistributed [1–3], which can lead to the instability of a roadway. Common failure modes for the surrounding rock include brittle failure, roof collapse, sidewall collapse [4–6], etc. The deep roadway is subjected to high stress, requiring excavation to confront complex stress conditions. The rock behaves in a completely different mechanical manner compared to shallow rock. Its strength characteristics, deformation mechanism, and damage mode are difficult to explain accurately using traditional theories [7,8]. How to effectively evaluate and maintain the safety of the surrounding rock has been a hot issue in the research of underground rock support engineering. The surrounding rock consists of the roof, floor, and sidewalls, and the stability of each component is of utmost importance. A prevalent method for examining the stability of a roadway is numerical simulation. The numerical simulation method can simulate complicated underground structures and geological conditions. This capability supports the investigation of parameter sensitivity and aids engineers in optimizing design schemes for underground engineering. The stress and strain in the surrounding rock after excavation are analyzed to determine the damage state of the roadway [9–12].

Most studies focus on the failure of roof rock and floor rock, while disregarding the significant contribution of the sidewall rock in maintaining the stability of a roadway. When damage occurs in the sidewall, it also means that the span of the roadway will

increase. Although the range of sidewall damage is limited, it should be noted that this limited damage range will trigger the overall failure of the roadway. As concluded by some scholars [13–15], it can result in a roof collapse or floor heave with the gradually increasing width of an underground excavation, which leads to the overall instability of the roadway. Małkowski et al. [16] proposed a numerical method to study the floor heave of roadways under dry and soaking conditions, and the obtained results were in good agreement with field measurement data. Coggan et al. [17] studied the influence of ground stress and rock layers on the safety of the surrounding rock and found that a weak roof rock layer is the main factor affecting the stability of a roadway. The failure types in sidewall rock include spalling, bursting, and folding [18,19]. Gou et al. [20] proposed that damage to sidewalls primarily results from tensile stress, which progressively transitions to shear damage as one moves toward the interior of a rock mass. Jia [21] analyzed some primary mechanical damage mechanisms of roadway sidewalls, categorizing the forms of roadway sidewall failure as compression-shear, gravity-slip, splitting, and transverse-arch. Wei et al. [22] simulated the stress of rock around coal roadways using a PFC two-dimensional numerical method. Ivan Sakhno and Svitlana Sakhno [23] suggested that rock failure begins at the corners of the bottom, progressively extending toward the bottom and sidewalls, ultimately leading to uncontrolled floor heaving in the roadway. With the transfer of concentrated stresses in the sidewalls to greater depths, the roof and floor are relatively stable and the sidewalls are gradually destroyed [24]. The plastic zone of surrounding rock near the sidewall is larger than that near the roof [25]. The serious damage of a roadway sidewall demonstrates that it is the key part that needs to be supported [26–29]. Local damage to the sidewall rocks can cause instability in the entire roadway, resulting in significant economic losses and even casualties. Therefore, it is important to avoid such damage to ensure the safe construction and use of deep underground coal mine roadway projects. Studying the deformation and damage mechanisms of sidewall rock is crucial to ensuring the safety of the surrounding rock in deep underground coal mining roadways.

In this paper, the analysis of the damage pattern of the sidewall rocks in the diabase roadway at the Datai coal mine is presented first. Following this, we will discuss a numerical model we have established. The model presents roadway systems in various conditions of height-width ratios and lateral pressure coefficients to analyze the evolving regulations of plastic damage, horizontal displacement, and vertical stress of sidewall rocks after excavation.

2. Project Overview

2.1. Failure Characteristics of Roadway Sidewalls

The Datai coal mine is located in the Mentougou District of Beijing, China. It has a strike length of 10.9 km, an inclined width of 0.67 km, and an area of 7.31 square kilometers. The surrounding rock of the roadway at the –410 m and –510 m horizontal levels of the Datai coal mine is composed of diabase, which is highly structurally dense and brittle. Additionally, it has a uniaxial compressive strength of 187 MPa, indicating a typical hard-rock geological condition. Based on the statistics of the fracture area of the highly brittle diabase rock roadway at the –410 m and –510 m levels in the Datai coal mine, the failure positions of the sidewall rock are shown in Figure 1.

The floor rock of the Datai coal mine is diabase, which is dark green to black in color, composed of plagioclase, hornblende, and other minerals, with a hard texture. The diabase fragment slices were observed using an electron microscope. It can be found that the diabase fracture is flat, the structure is dense, the grain boundary of the diabase particles is obvious, the damage is mostly intergranular fracture, and the brittle fracture characteristics are significant. The failure position of the surrounding rock mostly appears in the middle-upper or middle-lower part of sidewalls. The specific situation is shown in Figure 2. Large blocks of diabase fell from the roadway sidewall, forming a V-shaped destruction zone. The specific situation is shown in Figure 3. The rock roadway is about 800 m deep and is in a high in-situ stress state. Diabase is brittle, and the roadway sidewall is forced to deform

by the roof and bottom plate, which led to the main failure of the diabase in the roadway sidewall. The main cause of the damage was shear failure, and as it failed it formed a V-shaped rupture pit.

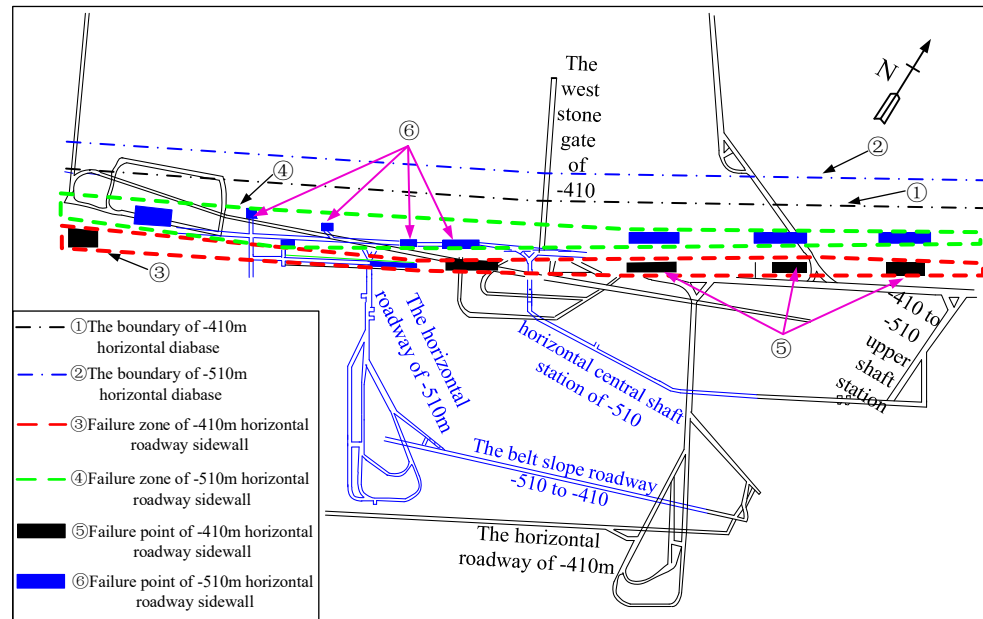


Figure 1. Distribution of roadway failure occurrence at the levels -410 m and -510 m in Datai coal mine.



Figure 2. Failure zone of the sidewall: (a) Middle-upper part of roadway sidewall; (b) Middle-lower part of roadway sidewall.

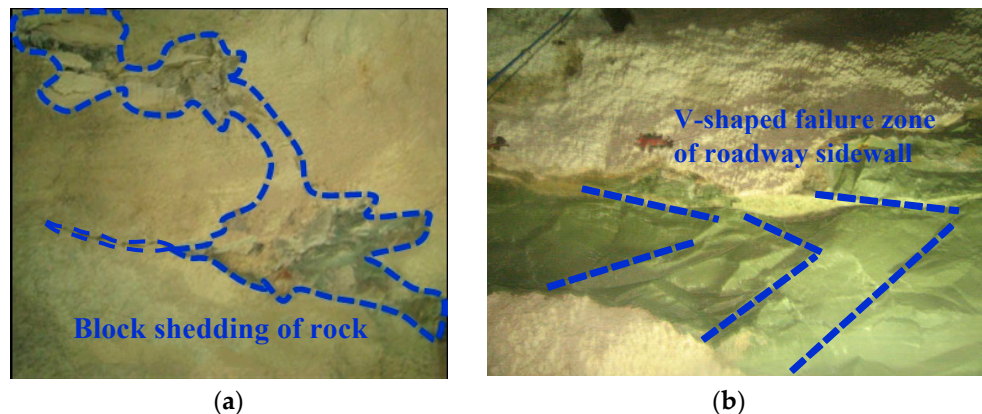


Figure 3. Failure characteristics of the roadway sidewall: (a) Block shedding; (b) Shape of destruction.

2.2. In-Situ Stress

The deep rock mass of the Datai coal mine is in an in-situ high stress environment, which leads to serious deformation of and damage to the roadway. In-situ stress is tested using the stress relief method [30]. The in-situ stress is measured from a distant point prior to the construction of the roadway. Two in-situ stress measuring points are set at the level of −510 m. The results of the in-situ stress test are illustrated in Table 1.

Table 1. The magnitude and direction of principal stress on each measuring location.

Number of Measuring Points	Principal Stress	Principal Stress Value (MPa)	Principal Stress Direction (°)	
			Azimuth Angle	Dip Angle
1	σ_1	45.69	154.91	−2.11
	σ_2	24.44	80.21	77.62
	σ_3	19.10	244.85	8.95
2	σ_1	49.30	156.79	−2.40
	σ_2	25.63	80.21	79.76
	σ_3	18.46	246.37	9.95

According to the results of the stress measurements performed on the Datai coal mine roadway at −510 m, the following conclusions can be obtained.

- (1) The azimuth angles of the principal stress σ_1 of the two measuring points are 154.91° (borehole 1) and 156.79° (borehole 2), respectively, values which are basically consistent with the principal stress direction in North China. Near east-west (the Datai coal mine is east of Taihang Mountain), the azimuth angle of borehole 2 is 224°, and the included angle with the azimuth angle of σ_1 is 67.21°. The core discing phenomenon appeared in borehole 2, as shown in Figure 4. This is a main feature of rock masses under high ground stress.
- (2) At the two measuring points, σ_1 had dip angles of −2.11° and −2.40°, respectively. σ_1 is oriented in a near-horizontal direction, suggesting that the in-situ stress in this area is mainly characterized by horizontal compressive stress. Therefore, it is necessary to study the effect of horizontal ground stress on the safety of the rock mass, which can be determined by changing the lateral pressure coefficient.
- (3) The principal stress values of the two measuring points in the near vertical direction are 24.44 MPa and 25.63 MPa, respectively, values which are basically equal to the pressure of the overlying strata per unit area at the −510 m level.
- (4) The differences between the dip angles of σ_1 and σ_3 at the two measuring points are 11.06° and 12.35°, respectively. The differences between the dip angles are small and similar to the horizontal direction. At the same time, σ_1 is 2.39~2.67 times the minimum principal stress σ_3 , and the difference is larger. Shear failure in the rock mass of a sidewall is serious.

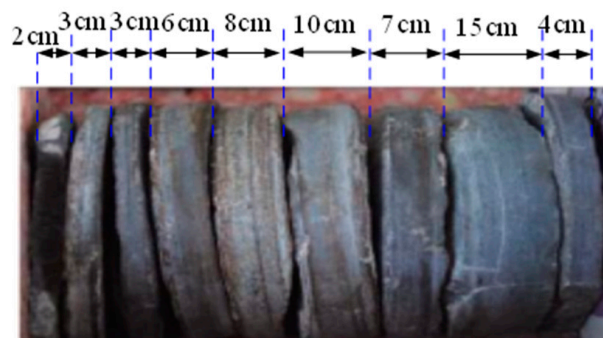


Figure 4. Core discing phenomenon in the borehole 2 of the roadway sidewall.

3. Materials and Methods

After unloading, the tiny unit at the boundary of sidewall rock is in a stress state of one face free and five faces loaded. Under this special stress state, its deformation and failure law are easily affected by external influences. The rock mass of the sidewall is prone to tensile failure and shear failure, which in turn causes a series of safety disasters. In this section, FLAC3D, a finite-difference-based method is used to establish a model of the Datai coal mine and study the deformation and destruction laws of diabase. A numerical model is used to simulate the displacement and destruction laws of the surrounding rock of the roadway sidewall under different influencing factors. The study content of this paper lays out a certain theoretical framework for a deep understanding of the destruction mechanism of brittle rock or coal rock and provides some suggestions for the reasonable development of rock support control technology for roadway sidewalls.

3.1. Model Size and Parameters

This paper studies a mining roadway located in a coal mine the working face in the Datai Coal Mine of China. It is rectangular and there is no cavity near it. The actual roadway has the characteristics of symmetry along the central axis of the cross section of the roadway in terms of lithology, roadway shape, and buried depth. This simulation takes the -410 m horizontal rock roadway of the coal seam floor of the Datai coal mine as the prototype, and the model takes half of the structure of the roadway for numerical simulation. The model grid division is shown in Figure 5. The size of the model and roadway is constantly changing, when we studied the influence of the height-width ratio on results. The method of selecting the size of the model was that the length of the fixed model is 60 m, the width of the fixed model is 40 m, the height of the fixed model is 40 m, and the width of the roadway is 4 m. When the height-width ratio of the roadway increases, the height of the roadway also increases. For example, when the height-width ratio takes the maximum value of 2, the half-height of the roadway takes the maximum value of 4 m, the distance between the upper boundary of the model and the center of the roadway is 20 m, and the ratio of the two is 5. Therefore, when studying the influence of the height-width ratio on results, the distance between the model boundary and the center of the roadway is at least 5 times greater than the maximum size of the roadway. When studying the influence of the lateral pressure coefficient on the results, the distance between the model boundary and the center of the roadway is always 10 times the maximum size of the roadway.

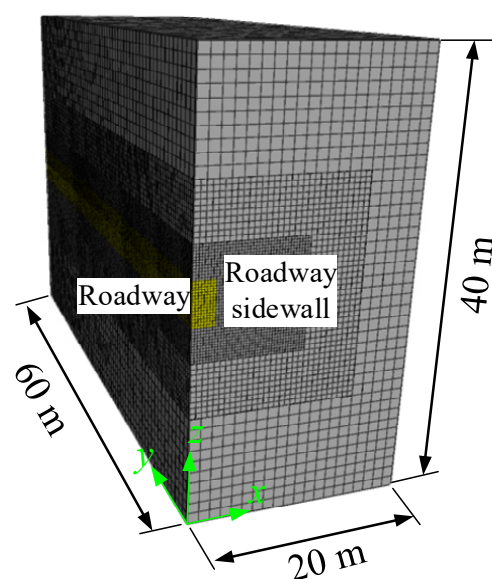


Figure 5. Three-dimensional model used for numerical calculation of roadway sidewall failure (height-width ratio $h/w = 1$).

The boundary conditions set in the numerical simulation are illustrated in Figure 6. The top part of the rock mass represents the formation load. The x-direction boundaries are fixed at both ends. The y-direction boundaries are fixed, and the lower end of the z-direction is also fixed. Horizontal stress is applied to the internal elements of the numerical model based on the lateral pressure coefficient.

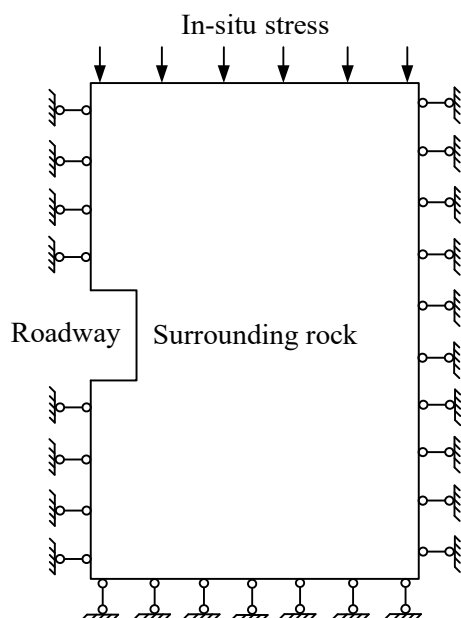


Figure 6. Boundary conditions used in rock mass.

In this simulation, the constitutive model adopts the Mohr-Coulomb model. The surrounding rock of the roadway is diabase. The main material properties of diabase are elastic modulus, Poisson's ratio, density, friction angle, and cohesion. In order to obtain these material properties, we made the rock samples taken in the field into standard specimens and carried out unit axial compression and triaxial tests. The mechanical properties of diabase are taken from the high brittle diabase of the coal seam floor of the Datai coal mine, as shown in Table 2. Among them, E is the Young's modulus of the diabase, ν is the Poisson's ratio of diabase, c is the cohesion of the diabase, and φ is the internal friction angle.

Table 2. Material properties of diabase in simulation.

Name	E (GPa)	ν	c (MPa)	φ (°)	ρ (g/cm ³)
Diabase	25	0.24	10	42	2.83

3.2. Simulation Scheme

First, the initial equilibrium of in-situ stress is calculated, and the displacement and velocity are cleared after the model is calculated to equilibrium. Regardless of the influences of the excavation method and support, the roadway of the model is excavated directly at one time, and the model is calculated until it balances.

Two simulation schemes are set up for the roadway height-width ratio h/w (the width is constant) and lateral pressure coefficient λ . Scheme 1: when the lateral pressure coefficient is 0.5, the internal friction angle is 42°, and the cohesion is 10 MPa. The simulated roadway height-width ratio varies between 0.25 and 2.0. Scheme 2: when the roadway height-width ratio is 1.0, φ is 42°, and c is 10 MPa, the simulated lateral pressure coefficient is 0.1~1.0. The specific study protocol is given in Table 3. During the simulation process, the data of the $y = 30$ m area of the roadway sidewall rock mass were monitored to obtain the horizontal displacement at the middle position of the roadway sidewall, tensile and

shear plastic zone depth of the sidewall, and the vertical stress change inside the rock mass of the roadway sidewall.

Table 3. Scheme design of simulation.

Scheme	Roadway Height-Width Ratio h/w	Lateral Pressure Coefficient λ
Scheme 1	0.25, 0.50, 0.75, 1.0, 1.25, 1.50, 1.75, 2.00	0.5
Scheme 2	1.0	0.1, 0.2, 0.3, 0.4, 0.5, 0.6, 0.7, 0.8, 0.9, 1.0

4. Results and Analysis

4.1. Influence of Roadway Height-Width Ratio

4.1.1. Plastic Damage Zone of Roadway Sidewall

The distribution of plastic areas in the rock masses of roadways with various roadway height-width ratios h/w is illustrated in Figure 7. As shown in the figure, as the h/w ratio increases, the distribution height and width range of the tensile and shear plastic rock around the roadway sidewall are increasing. When the h/w is small, the tensile plastic zone is a circular arc. When the h/w is large, the tensile plastic zone is also arc-shaped, but it is approximately V-shaped, while the shear plastic zone appears as a circular arc. Importantly, the increase in the height-width ratio of the roadway results in a more significant change in the area of the plastic failure zone of the roadway compared to the roof and floor. This observation highlights the notable impact of the roadway's height-width ratio on the stability of the roadway sidewall. Therefore, the rational design of the h/w of a roadway should be carried out in the design stage, before construction.

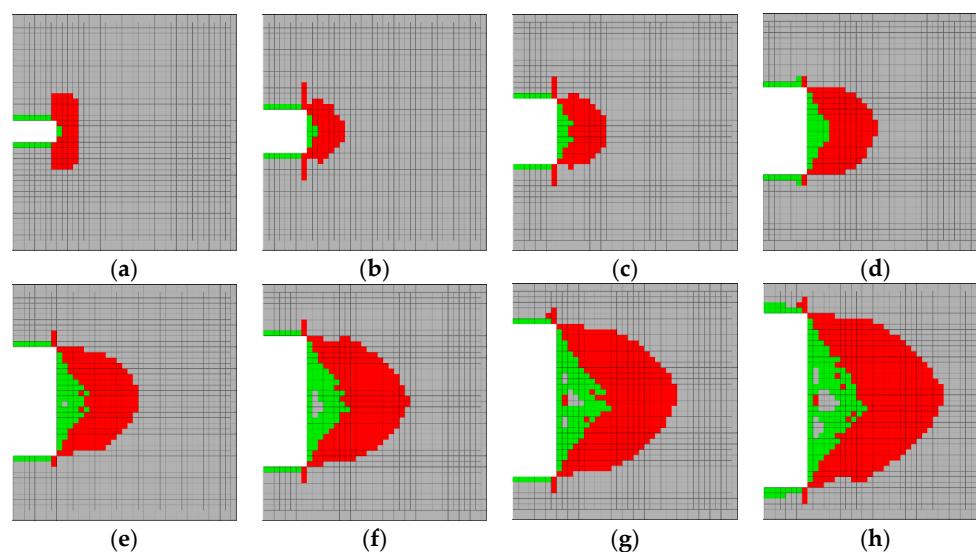


Figure 7. Distribution of tensile and shear plastic zones in roadway sidewall under various height-width ratio h/w (green is tensile and red is shear): (a) $h/w = 0.25$; (b) $h/w = 0.50$; (c) $h/w = 0.75$; (d) $h/w = 1.00$; (e) $h/w = 1.25$; (f) $h/w = 1.50$; (g) $h/w = 1.75$; (h) $h/w = 2.00$.

The range of change of the tensile and shear plastic areas of rock masses of different height-width ratios is illustrated in Figure 8. The width of the tensile and shear plastic area increases linearly as the roadway's h/w becomes larger. Under different roadways' h/w , especially when the roadway height-width ratio is small, the area of the shear plastic zone of a roadway rock mass is generally greater than that of the tensile plastic area. For example, when $h/w = 0.25$, the depth of the shear plastic zone is about three times that of the tensile plastic zone. When $h/w = 2.00$, the width of the shear plastic area is about 1.45 times that of the tensile plastic area. From the perspective of the forming process of the plastic area of surrounding rock, a sidewall is damaged first by tensile stress and then by shear damage, but the final roadway failure is mainly a shear failure.

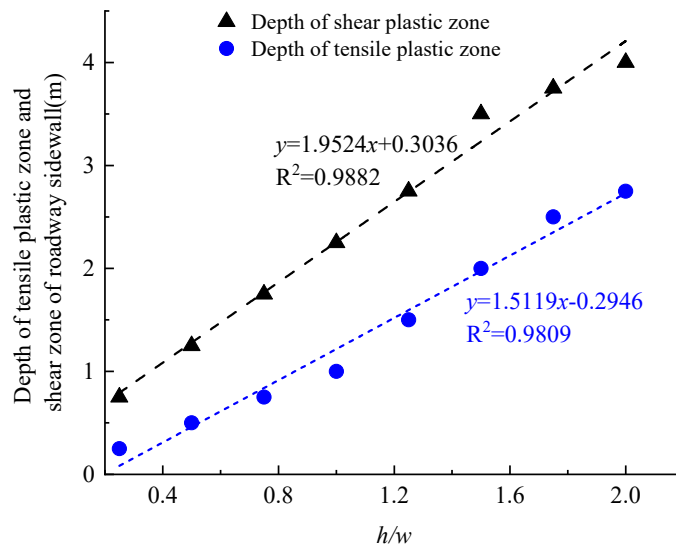


Figure 8. Scatter of the relationship between h/w and the depth of the tensile plastic zone and shear plastic zone of a roadway sidewall.

4.1.2. Horizontal Displacement of Roadway Sidewall

The relation between the height-width ratio h/w of a roadway and the maximum horizontal displacement of the roadway’s sidewall is illustrated in Figure 9. As the roadway’s height-width ratio h/w increases, the horizontal displacement of the roadway sidewall increases linearly. For each unit increase in the roadway’s h/w , the maximum horizontal displacement of the roadway sidewall increases by about 11.33 mm. For example, when $h/w = 0.25$, the deformation of the sidewall is small, only 1.99 mm. When $h/w = 2.00$, the deformation of the sidewall increases to 22.21 mm. It can be seen that the effect of the height-width ratio h/w of a roadway on the displacement of the rock mass of the roadway is obvious. Therefore, we should provide timely and effective support for a roadway with significant damage and deformation in the field.

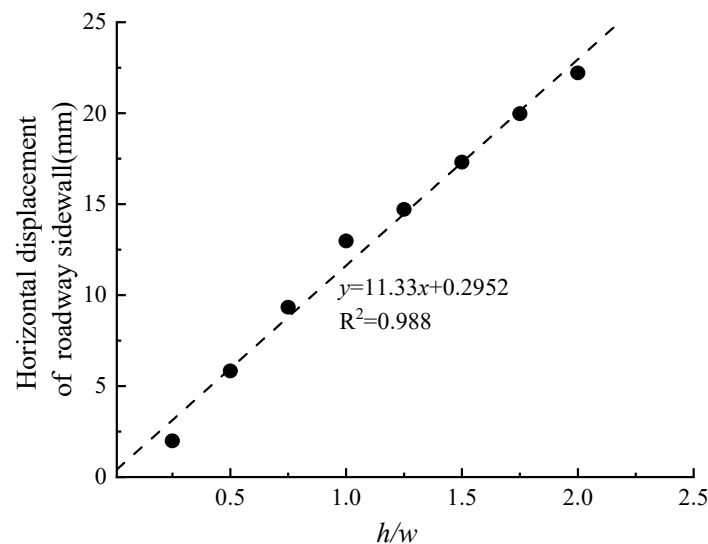


Figure 9. Relationship between h/w and horizontal displacement of the roadway sidewall.

4.1.3. Vertical Stress of Roadway Sidewall

The vertical stress distribution of various roadway aspect ratios h/w is depicted in Figure 10. As the height-width ratio h/w of a roadway increases, the area affected by the excavation disturbance gradually expands. Consequently, both the stress release zone and areas with high stress values expand accordingly. The areas with high vertical stress values

in the sidewall rock mass moves to the deeper surrounding rock area, ultimately resulting in two extreme stress points forming within the deeper rock mass area of the roadway.

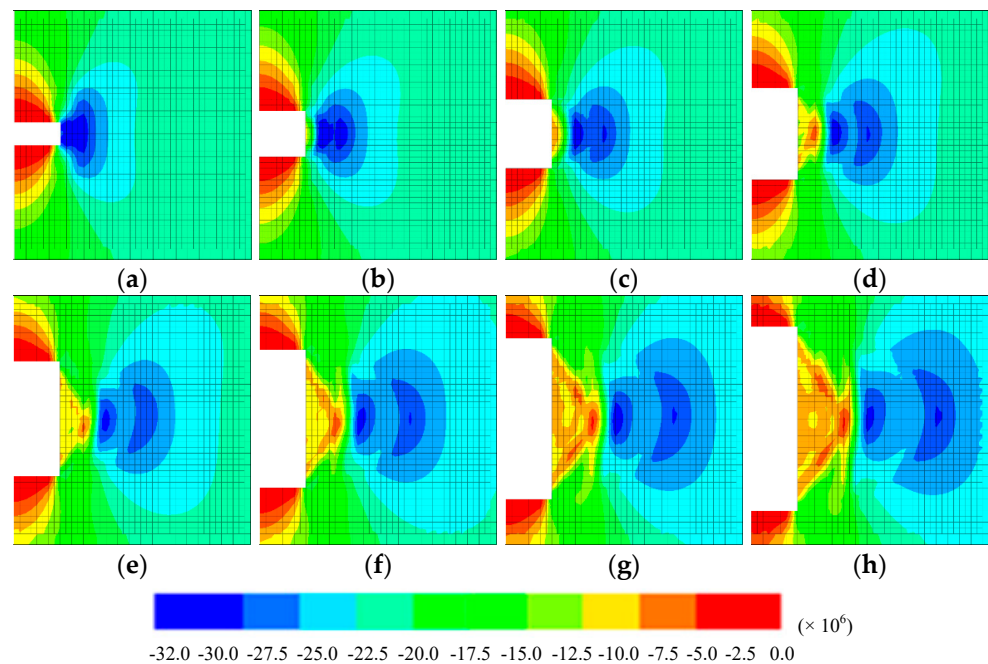


Figure 10. Vertical stress of sidewall under various height-width ratio h/w (green is tensile and red is shear): (a) $h/w = 0.25$; (b) $h/w = 0.50$; (c) $h/w = 0.75$; (d) $h/w = 1.00$; (e) $h/w = 1.25$; (f) $h/w = 1.50$; (g) $h/w = 1.75$; (h) $h/w = 2.00$.

The variation of vertical stresses inside a sidewall with increasing distance from the boundary of the roadway sidewall is illustrated in Figure 11. Initially, as the distance from the sidewall boundary increases, the vertical stress escalates swiftly until it reaches a peak. Subsequently, it undergoes a slight decline before gradually ascending to a second peak, followed by a gradual decrease and eventual stabilization. When h/w is small, for example, when $h/w = 0.25$, the vertical stress inside the sidewall has only one stress concentration point. With the increase of h/w to 0.75, two vertical stress concentration points appear inside the roadway sidewall. As h/w continues to increase from 0.75, the second stress peak gradually rises, eventually approaching the value of the first stress peak.

The relationship between h/w and maximum vertical stress inside of a roadway sidewall is shown in Figure 12. When h/w increases from 0.25 to 0.50, the vertical stress value at the first stress concentration point is rapidly reduced from 41.5 MPa to 33.07 MPa. The vertical stress decreases slowly, and then increases slightly. When $h/w = 0.25$, the vertical stress changes to 31.35 MPa. In general, the stress value of the first stress concentration point inside a roadway sidewall first decreases and then increases as the height-width ratio h/w of the roadway rises, showing a secondary polynomial relationship. As the height-width ratio h/w of the roadway rises, the stress concentration point moves progressively deeper into the surrounding rock. When h/w was increased from 0.25 to 2.00, several notable changes occurred. First, the distance between the stress concentration position and the roadway sidewall increased from 0.5 m to 3.27 m. The distance between the maximum stress concentration point and boundary of the sidewall rock mass and the aspect ratio h/w of the roadway increase linearly. Additionally, the stress value at the second stress concentration point showed an increase with the rising roadway's h/w , exhibiting a quadratic polynomial relationship. Furthermore, as the h/w ratio increased, the stress concentration position shifted gradually deeper into the rock mass. Specifically, when the h/w ratio was increased from 0.25 to 2.00, the distance between the vertical stress concentration position and the roadway sidewall extended from 0.75 m to 6.25 m. The

stress concentration position has a linear growth relationship with the roadway sidewall distance and the roadway height-width ratio h/w .

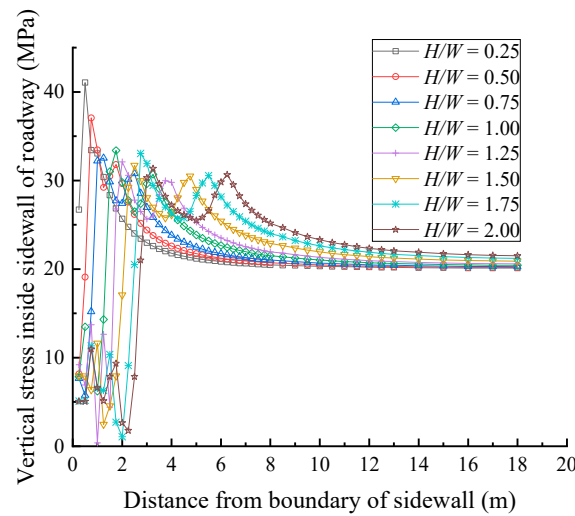


Figure 11. Vertical stress monitoring curves inside the sidewall of the roadway under different h/w .

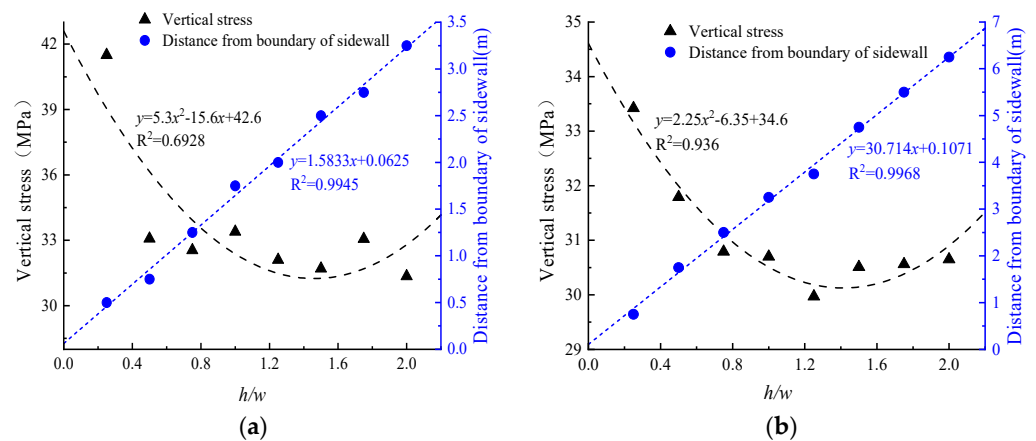


Figure 12. Relationship between h/w and maximum vertical stress inside of the roadway sidewall: (a) First stress peak point inside of roadway sidewall; (b) Second stress peak point inside of roadway sidewall.

4.2. Influence of Lateral Pressure Coefficient

4.2.1. Plastic Damage Zone of Roadway Sidewall

Figure 13 illustrates the distribution of the tensile shear plastic area in the rock mass of a sidewall under varying λ values. As the λ increases, the extent of the tensile plastic zone at the roof and floor of the roadway initially decreases before eventually increasing. The shape of the failure zone in the surrounding rock transitions from an X shape to a V shape, with the failure zone of the roadway side consistently displaying a substantial range. Furthermore, the increase in λ results in noticeable changes in the plastic failure area of the roof, floor, and roadway sidewall. This underscores the significant role of the λ in influencing roadway stability. Therefore, it is crucial to conduct ground stress measurements and estimations during the roadway support design phase to implement effective support measures.

The range of tensile and shear plastic areas in the middle of rock mass varies with λ value is illustrated in Figure 14. With the rise of λ value, the range of the tensile plastic area in a roadway sidewall's surrounding rock first decreases and then basically remains unchanged. The λ value has a quadratic polynomial relationship with the depth of the

tensile plastic area. With the rise of the λ value, the range of the shear plastic area of the surrounding rock of the sidewall first increases and then decreases. When λ increases from 0.1 to 0.3, the range of the shear plastic zone increases from 2.0 m to 2.75 m (maximum). When λ increases from 0.3 to 1.0, the depth of the shear plastic region decreases to 1.5 m.

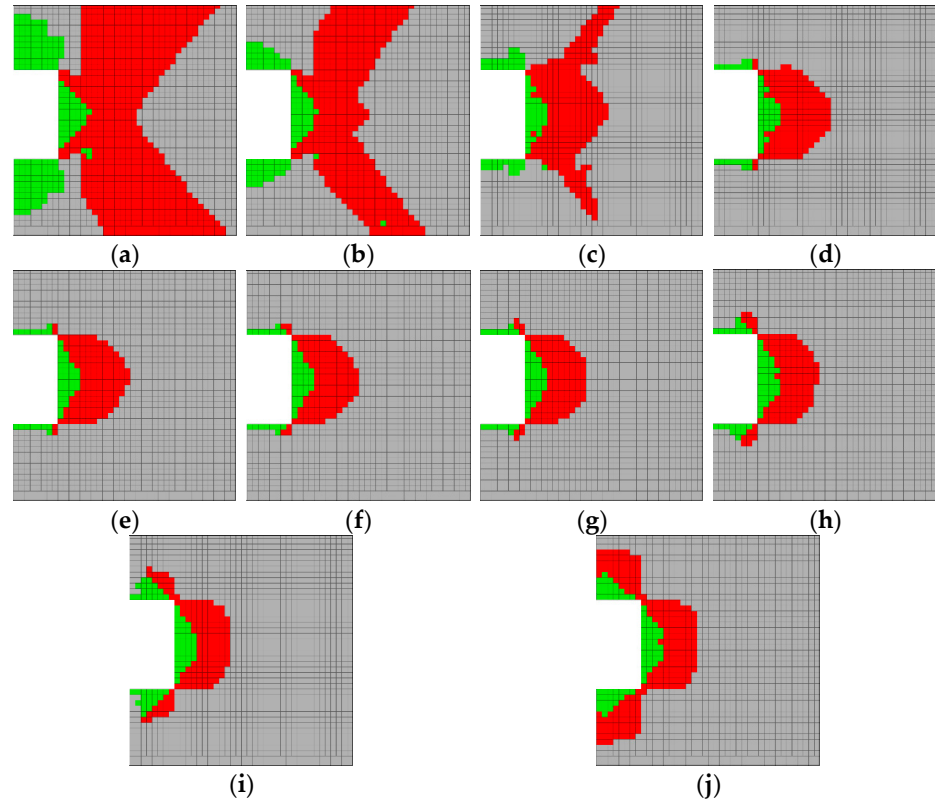


Figure 13. Distribution of tensile and shear plastic zones in the roadway sidewall under different lateral pressure coefficients λ (green is tensile and red is shear): (a) $\lambda = 0.1$; (b) $\lambda = 0.2$; (c) $\lambda = 0.3$; (d) $\lambda = 0.4$; (e) $\lambda = 0.5$; (f) $\lambda = 0.6$; (g) $\lambda = 0.7$; (h) $\lambda = 0.8$; (i) $\lambda = 0.9$; (j) $\lambda = 1.0$.

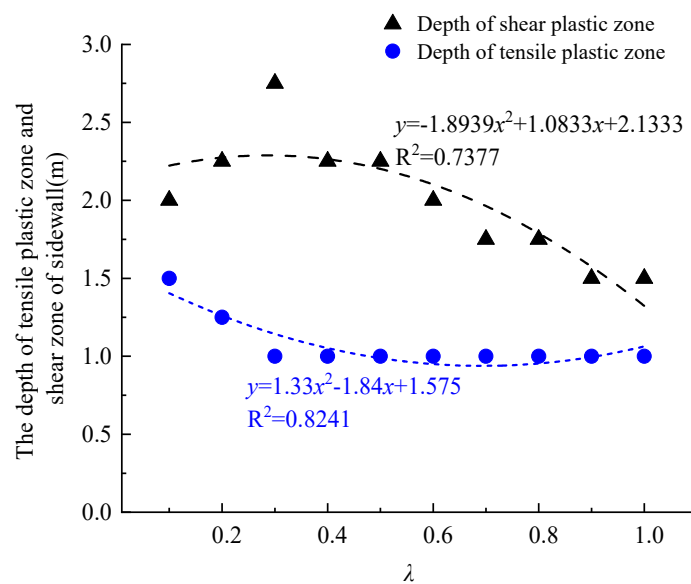


Figure 14. Scatter of the relationship between the λ and the depth of tensile plastic zone and shear zone of the roadway sidewall.

4.2.2. Horizontal Displacement of the Roadway Sidewall

The horizontal displacement distribution of a rock mass varies with the λ value, as illustrated in Figure 15. As the λ value increases, the horizontal displacement of the sidewall of a roadway first decreases and then rises. With a λ value of 0.1, the corresponding horizontal displacement of a roadway sidewall reaches the value of 22.15 mm. When the λ value rises to 0.3, the horizontal displacement of a roadway sidewall is reduced to 12.66 mm. When the λ value increases to 0.5, the horizontal displacement of the roadway sidewall fluctuates up and down to 12.98 mm. The horizontal displacement increases as the λ value continues to increase from 0.5. When the λ value rises to 1.0, the horizontal displacement of the roadway sidewall rises to 19.57 mm. In general, the horizontal displacement and lateral pressure coefficient of the roadway sidewall show a quadratic polynomial relationship.

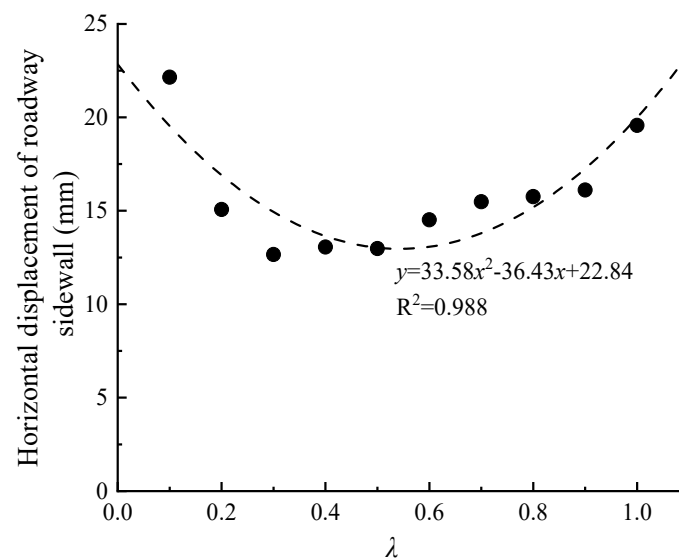


Figure 15. Relationship between λ and horizontal displacement of the roadway sidewall.

4.2.3. Vertical Stress of Roadway Sidewall

Figure 16 shows the vertical stress distribution of the rock mass of a sidewall under various λ values. With the rise of the λ value of the roadway, the vertical stress concentration range of the rock mass of the roadway sidewall is close to the roadway side, and the stress concentration in the roadway side is higher than that of other parts. Areas with high vertical stress values near the roof and floor and the roadway side also gradually shift into the shallow surrounding rock with the rise of lateral pressure.

Under varying λ values, with the rise of the distance from the boundary of the roadway sidewall, the evolution pattern of vertical stress inside a roadway is illustrated in Figure 17. Taking the λ value equal to 0.5 as an example, vertical stress at the roof of the roadway at 3 m away from the roadway sidewall reaches 26.16 MPa. The internal vertical stress equals 33.39 MPa at 1.75 m from the boundary of sidewall. When 3.25 m from the roadway sidewall, vertical stress reaches the second peak of 30.7 MPa.

The relationship between the λ value and the internal stress distribution of a sidewall rock mass is shown in Figure 18. The stress value at the first stress concentration point in the rock mass decreases with the rise of λ value. The position of the stress concentration point gradually shifts to the roadway sidewall with the rise of the λ value. The stress value of the second stress concentration first increases and then decreases with the rise of the λ value. For instance, at a λ value of 0.2, the vertical stress measures 27.01 MPa. Subsequently, as the λ value escalates from 0.2 to 0.5, the vertical stress ascends to 30.7 MPa. However, with a further increase in the λ value from 0.5 to 1.0, the vertical stress gradually declines to 29.3 MPa. In general, the distance between the stress concentration position and the roadway's side decreases slowly and linearly with the augmentation of the λ value.

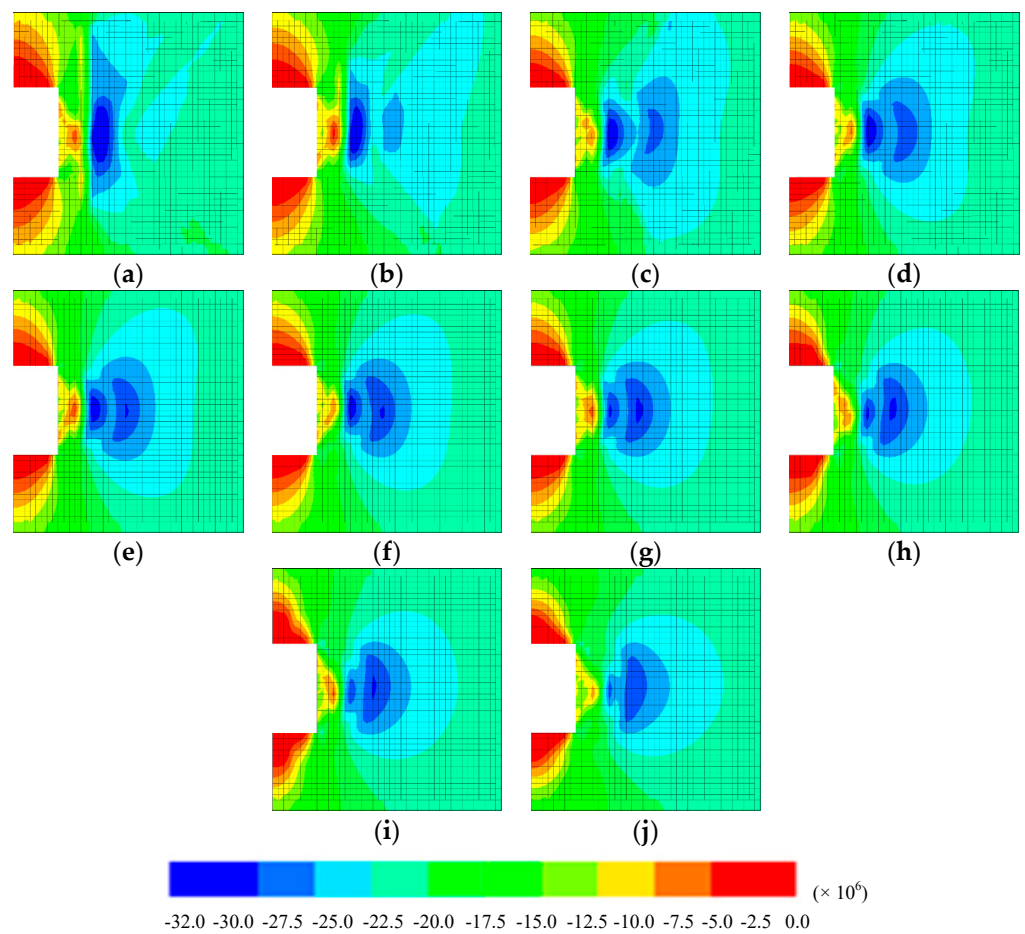


Figure 16. Vertical stress distribution in the roadway sidewall under different lateral pressure coefficient λ (green is tensile and red is shear): (a) $\lambda = 0.1$; (b) $\lambda = 0.2$; (c) $\lambda = 0.3$; (d) $\lambda = 0.4$; (e) $\lambda = 0.5$; (f) $\lambda = 0.6$; (g) $\lambda = 0.7$; (h) $\lambda = 0.8$; (i) $\lambda = 0.9$; (j) $\lambda = 1.0$.

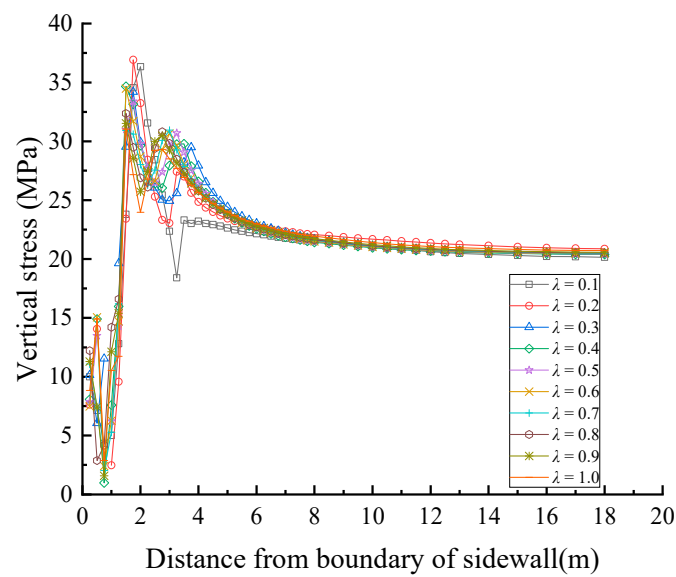


Figure 17. Vertical stress monitoring curves inside the sidewall of the roadway under different λ .

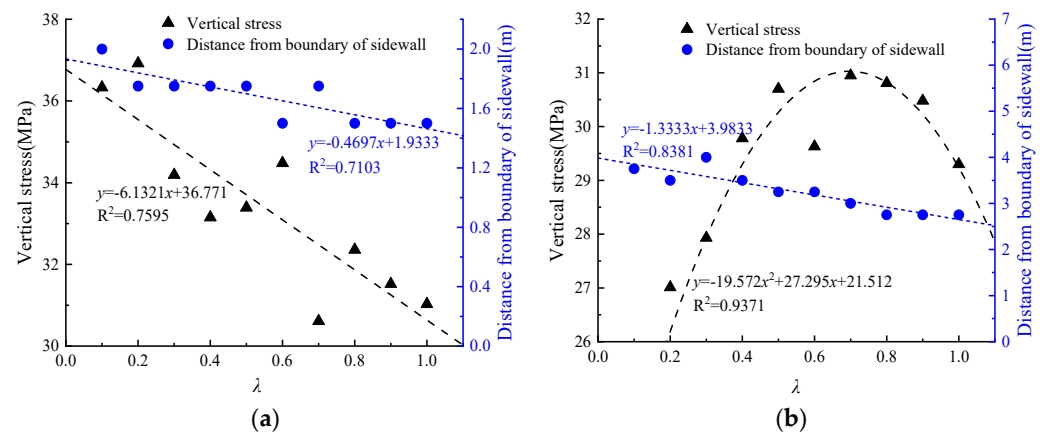


Figure 18. Relationship between λ and maximum vertical stress inside of the roadway sidewall: (a) First stress peak point inside of roadway sidewall; (b) Second stress peak point inside of sidewall.

5. Conclusions

In this paper, the effects of the roadway height-width ratio and lateral pressure coefficient on the plastic damage zones, horizontal displacements, and stress changes in the roadway sidewalls were investigated. The purpose was to study the brittle damage mechanisms of highly stressed roadway sidewalls. The following conclusions were drawn.

- (1) The rock surrounding the roadway of the Datai coal mine is under high in-situ stress, and the diabase is dense and brittle. The roadway sidewall damage mostly occurs in the upper middle or middle-lower part, mainly as shear failures, forming a large falling block fissure with a wide range, and finally forming a V-shaped failure zone.
- (2) When the height-width ratio of the roadway increases from 0.25 to 2.00, the tensile and shear plastic zones of the roadway sidewall gradually expand. The tensile plasticity damage zone is V-shaped, and the shear plasticity damage zone is circular. In addition, the shear plastic damage zone is larger than the tensile plastic damage zone. The vertical stress in the roadway sidewall experiences two peaks. The stress decreased slightly between the peaks, and then gradually decreased and stabilized. It was found that the horizontal displacement of the roadway sidewall increased linearly. With the rise of the roadway height-width ratio h/w , the values of the two peaks get closer and closer. The stress at the two stress concentration points increases and then decreases, and the stress concentration location is gradually shifted to a deeper part of the roadway sidewall.
- (3) As the λ value increases from 0.1 to 1.0, the tensile plastic damage area of the roadway sidewall first decreases and then remains unchanged, and the shear plastic damage zone first increases and then decreases. The horizontal displacement of the roadway sidewall shows a trend of decreasing and then increasing. The vertical stress within the roadway sidewall increases at the first peak point, then decreases slightly, and then continues to increase to the second peak point. The stress value decreases linearly at the first stress concentration point and tends to increase and then decrease at the second stress concentration point. Then it gradually decreases and stabilizes. The stress value decreases linearly at the first stress concentration point and tends to increase and then decrease at the second stress concentration point. It is worth noting that these two stress concentration locations are shifted to the boundary of the roadway sidewall.

Author Contributions: Conceptualization, X.W. and Y.Z.; methodology, Y.Z.; software, M.X.; validation, J.F.; formal analysis, B.J.; investigation, J.F.; writing—original draft preparation, X.W. and B.J.; writing—review & editing, Y.Z.; supervision, Y.Z. and M.X. All authors have read and agreed to the published version of the manuscript.

Funding: This research was funded by National Natural Science Foundation of China (No. 52104137), Major Program of Shandong Provincial Natural Science Foundation (No. ZR2019ZD13) and Shandong Provincial Natural Science Foundation (No. ZR2020QE122).

Institutional Review Board Statement: Not applicable.

Informed Consent Statement: Not applicable.

Data Availability Statement: The data of this work can be shared to the readers depending on the request.

Conflicts of Interest: The authors declare no conflicts of interest.

References

1. Yi, X.; Gao, F.; Liu, X. Permeability and pressure distribution characteristics of the roadway surrounding rock in the damaged zone of an excavation. *Int. J. Min. Sci. Technol.* **2017**, *27*, 211–219.
2. Gong, W.; Peng, Y.; He, M.; Xie, T.; Zhao, S. An overview of the thermography-based experimental studies on roadway excavation in stratified rock masses at CUMTB. *Int. J. Min. Sci. Technol.* **2015**, *25*, 333–345. [[CrossRef](#)]
3. Sun, X.; Wang, D.; Feng, J.; Zhang, C.; Chen, Y. Deformation control of asymmetric floor heave in a deep rock roadway: A case study. *Int. J. Min. Sci. Technol.* **2014**, *24*, 799–804. [[CrossRef](#)]
4. Wang, H.; He, S. Stability analysis of surrounding rock of shallow-buried subway tunnel with small spacing under different working conditions. *Geotech. Geol. Eng.* **2022**, *40*, 5065–5079. [[CrossRef](#)]
5. Gao, B.; Yang, C.; Li, L.; Zhang, H.; He, W.; Yang, Z.; Cai, Z. Surrounding rock failure mechanism and long-term stability of the heidong large ancient underground caverns. *Geotech. Geol. Eng.* **2022**, *40*, 4975–4990. [[CrossRef](#)]
6. Mangal, A. Strata Stability Investigation and Convergence Monitoring (SSICM) in Thick-Seam Depillaring with Caving by Cable Bolting Method. *Min. Metall. Explor.* **2021**, *38*, 927–944. [[CrossRef](#)]
7. Cao, R.; Cao, P.; Lin, H. Support technology of deep roadway under high stress and its application. *Int. J. Min. Sci. Technol.* **2016**, *26*, 787–793. [[CrossRef](#)]
8. Karolina, A.-P.; Daniel, P. Influence of driving direction on the stability of a group of headings located in a field of high horizontal stresses in the polish underground copper mines. *Energies* **2021**, *14*, 5955. [[CrossRef](#)]
9. Wu, X.; Wang, S.; Gao, E.; Li, C.; Ji, C.; Ma, S.; Li, T. Failure mechanism and stability control of surrounding rock in mining roadway with gentle slope and close distance. *Eng. Fail. Anal.* **2023**, *152*, 107489. [[CrossRef](#)]
10. Shi, J.; Feng, J.; Peng, R.; Zhu, Q. The research on stability of surrounding rock in gob-side entry driving in deep and thick seam. *Geotech. Geol. Eng.* **2022**, *40*, 3357–3364.
11. Chen, C.; Liu, Y.; Lou, H.; Jia, T. Stability control of a roadway surrounding rock during the cutting and pressure relief of a coal-bearing roof at a shallow mining depth. *Geofluids* **2022**, *2022*, 5308530.
12. Jia, X. Numerical simulation of the stability of deep roadway surrounding rock based on FLAC3D. In Proceedings of the International Conference of Green Buildings and Environmental Management, Qingdao, China, 5–7 June 2020.
13. Zhu, D.; Wu, Y.; Liu, Z.; Dong, X.; Yu, J. Failure mechanism and safety control strategy for laminated roof of wide-span roadway. *Eng. Fail. Anal.* **2020**, *111*, 104489. [[CrossRef](#)]
14. Hu, Y.; Liu, Y.; Shi, L. Research on Supporting Technology for Surrounding Rock of Inclined Large-Span Open-Off Cut Roadway. *Geotech. Geol. Eng.* **2020**, *38*, 1873–1884. [[CrossRef](#)]
15. Li, G.; He, M.; Zhang, G.; Tao, Z. Deformation mechanism and excavation process of large span intersection within deep soft rock roadway. *Int. J. Min. Sci. Technol.* **2010**, *20*, 28–34. [[CrossRef](#)]
16. Małkowski, P.; Ostrowski, Ł.; Stasica, J. Modeling of floor heave in underground roadways in dry and waterlogged conditions. *Energies* **2022**, *15*, 4340. [[CrossRef](#)]
17. Coggan, J.; Gao, F.; Stead, D.; Elmo, D. Numerical modelling of the effects of weak immediate roof lithology on coal mine roadway stability. *Int. J. Coal Geol.* **2012**, *90*, 100–109. [[CrossRef](#)]
18. Sun, X.; Chen, F.; Miao, C.; Song, P.; Li, G.; Zhao, C.; Xia, X. Physical modeling of deformation failure mechanism of surrounding rocks for the deep-buried tunnel in soft rock strata during the excavation. *Tunn. Undergr. Space Technol.* **2018**, *74*, 247–261. [[CrossRef](#)]
19. Fang, X.; He, J.; Li, H. A study of the rib fall mechanism in soft coal and its control at a fully-mechanized top-coal caving face. *J. China Univ. Min. Technol.* **2009**, *38*, 640–644. (In Chinese)
20. Gou, P.; Chen, Q.; Wu, T. Stability analysis of two sides of roadway supported with bolts. *J. Jiaozuo Inst. Technol.* **1999**, *18*, 317–321. (In Chinese)
21. Jia, J. Study on the failure style and its control method of soft ribs. *J. Taiyuan Univ. Technol.* **2005**, *36*, 93–95. (In Chinese)
22. Wei, J.; Wang, S.; Zhao, Z.; Li, D.; Guo, L. Numerical study of damage to rock surrounding an underground coal roadway excavation. *Adv. Civ. Eng.* **2020**, *2020*, 8863289. [[CrossRef](#)]
23. Sakhno, I.; Svitlana, S. Numerical studies of floor heave control in deep mining roadways with soft rocks by the rock bolts reinforcement technology. *Adv. Civ. Eng.* **2023**, *2023*, 2756105. [[CrossRef](#)]

24. Wu, D.; Qin, S. Loose and broken distribution of soft coal-rock in deep coal roadway sidewall. *Geotech. Geol. Eng.* **2020**, *38*, 4939–4948. [[CrossRef](#)]
25. Liu, S.; Zhang, H.; Zhang, W. Slipping hazard analysis and engineering application in up-right-side coal body of roadway for the incline coal seams. *Int. J. Min. Sci. Technol.* **2011**, *40*, 14–17. (In Chinese)
26. Yuan, W.; Hong, K.; Liu, R.; Ji, L.; Meng, L. Numerical simulation of coupling support for high-stress fractured soft rock roadway in deep mine. *Adv. Civ. Eng.* **2022**, *2022*, 7221168. [[CrossRef](#)]
27. Shi, Y.; Wang, H.; Tan, X.; Jin, Y.; Wang, J.; Tang, B. A stability analysis of an abandoned gypsum mine based on numerical simulation using the itasca model for advanced strain softening constitutive model. *Appl. Sci.* **2023**, *13*, 12570. [[CrossRef](#)]
28. Li, A.; Liu, Y.; Dai, F.; Liu, K.; Wang, K. Deformation mechanisms of sidewall in layered rock strata dipping steeply against the inner space of large underground powerhouse cavern. *Tunn. Undergr. Space Technol.* **2022**, *120*, 104305. [[CrossRef](#)]
29. Shan, R.; Kong, X.; Wei, Z.; Li, M.; Yang, S.; Tian, L. Theory and application of strong support for coal roadway sidewall. *J. Rock Mech. Geotech. Eng.* **2013**, *32*, 1304–1314. (In Chinese)
30. Simone, S. Validation and practical application of a data reduction software for the analysis of data from stress relief tests. *Geotech. Geol. Eng.* **2022**, *40*, 3779–3797.

Disclaimer/Publisher’s Note: The statements, opinions and data contained in all publications are solely those of the individual author(s) and contributor(s) and not of MDPI and/or the editor(s). MDPI and/or the editor(s) disclaim responsibility for any injury to people or property resulting from any ideas, methods, instructions or products referred to in the content.